Journal of Materials Chemistry C

ARTICLE

Poly(3-hexylthiophene)/Graphene Composites based Aligned Nanofibers for High Performance Field Effect Transistors

Chih-Jung Lin,[a] Cheng-Liang Liu[b] and Wen-Chang Chen[a],*

We report the morphology and field effect transistor (FET) characteristics of aligned electrospun nanofibers prepared from poly(3-hexylthiophene) (P3HT)/graphene composites. The graphene flake was more uniformly distributed in the nanofibers compared to that of spin-coated films, leading to different FET characteristics. The geometrical confinement from electrospun nanofibers could result in an enhanced π-π molecular packing with highly ordered orientation and reduce grain boundary during the strong stretching force, thereby increasing carrier mobility. The graphene behaved as the electronically conducting bridge between the P3HT domains in the composites and thus the FET mobility was generally enhanced as the graphene composition increased. Remarkably, the **ES-PG4** FET had a highest hole mobility of 1.82 cm^2 V^{-1} s^{-1} and moderately high I_{ON}/I_{OFF} of 5.88×10^4, which also exhibited good environmental stability for their transfer characteristics. The experimental results indicated that semiconducting composites based one-dimensional nanofiber devices offered the advantageous over the conventional spin-coated thin films and provided a simple strategy to produce high performance FET devices.

Introduction

Solution-processable semiconducting polymers have attracted an extensive research interest in electronic and optoelectronic device applications, such as light-emitting diode, photovoltaic cell, memory, field-effect transistor (FET), etc.[1-7] It was found that conjugated polymers could be constructed into one-dimensional structures with strong π-π interaction along the longitudinal axis for enhancing charge transporting characteristics.[8-10] For example, electrospinning is a simple and versatile technique for producing continuous, uniform and ultrafine one dimensional (1D) polymer nanofibers.[11-14] The elongated electrospun nanofibers of conjugated polymers by the strong shear forces form the interconnected π-π molecular stacking and ordered orientation of crystallines.[15-18] It thus promoted charge transport and reduced the grain boundary for increasing the carrier mobility in FET devices.[18-26]

Conjugated polymers based composites provide the possibility to improve the physical properties for device applications. For example, the combination of polymers with carbonaceous materials could significantly enhance the mechanical, thermal and electrical properties,[27-32] such as graphene nanofiller materials. In addition, the composite thin films of semiconducting polymers (such as poly(3-hexylthiophene) (P3HT)) and graphene exhibited an increase in the overall charge carrier mobilities due to the preferential paths for charge transport.[33-38] However, the above composites were characterized in the thin film, not in the 1D nanostructure, such as nanofibers. It is anticipated that the unique properties could be observed from the synergistic effect on the nanofibers and graphene/polymer nanocomposites.[8] However, the superior control over the size and uniformity of nanofiber-based conjugated polymer composites for the device applications are still challenging.

In this study, we fabricate aligned electrospun nanofibers from P3HT/graphene composites as the nanoscale channel for organic field effect transistor applications. The morphological and electrical properties of different graphene composition into P3HT nanofiber matrix (**ES-PGX**; **X**=1~5, referred to 0, 4.8, 10.7, 19.4, 25.4 and 31.7 wt% of graphene in P3HT) were discussed and compared to those based on pristine P3HT. Besides, the corresponding spin-coated nanocomposite thin films (**SC-PGX**; **X**=1~5) were also fabricated for comparison. The experimental results suggested these combined P3HT/graphene composite nanofibers had a superior performance in FET devices compared to those of pristine P3HT or thin film phase.

[a] Department of Chemical Engineering, National Taiwan University, Taipei, 10617 Taiwan. E-mail: chenwc@ntu.edu.tw

[b] Department of Chemical and Materials Engineering, National Central University, Taoyuan, 32001 Taiwan.

† Electronic Supplementary Information (ESI) available: See DOI: 10.1039/b000000x/

This journal is © The Royal Society of Chemistry 2015

J. Mater. Chem. C, 2015, **XX**, X-X | 1
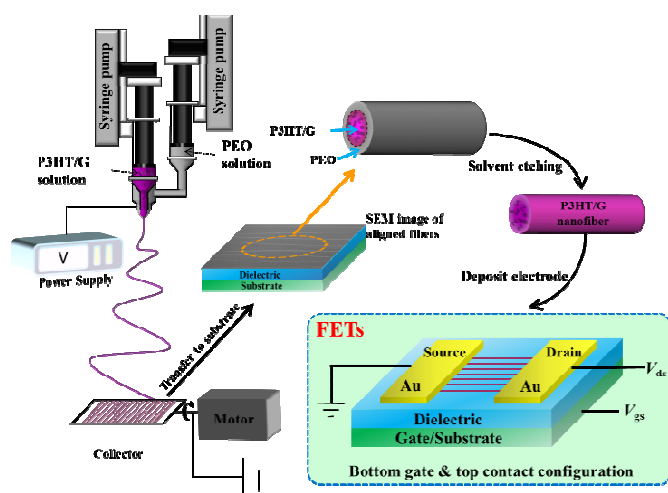
Fig. 1 Schematic illustration of electrospinning process for producing P3HT/graphene composite nanofibers and their FET device configuration.

Experimental Section

Materials

All commercially available reagents or solvents obtained from suppliers were used without further purification. P3HT ($M_w \sim$ 50,000 g mol^{-1}, 90-95% regioregularity) was received from Rieke Metals Inc. (USA). Poly(ethylene oxide) (PEO; M_w = 400,000 g mol^{-1}), octadecyltrichlorosilane (ODTS), chlorobenzene (CB; anhydrous 99.8%) and cyclohexane (CH; anhydrous 99.5%) were purchased from Aldrich (USA). A few layers of graphene nanopowder (3 nm flake size, black powder) were delivered from Graphene Supermarket (USA). Tetrabutylammonium perchlorate (TBAP) was purchased from TCI (Japan)

Preparation of P3HT/graphene (PGX) blend solutions

The P3HT/graphene blend solutions (**PGX**, **X**=1~5) were prepared using polymer-assisted dispersion method. P3HT and graphene were separately dissolved in chlorobenzene under sonication with an ultrasonicator and gentle shaking. The relevant quantity of P3HT is then added to graphene dispersion and the mixture was again sonicated. After sonication, the blend dispersion was centrifuged to allow the large aggregates to sediment. The supernatants from the top portions were used as P3HT/graphene blend solutions referred to **PG0**, **PG1**, **PG2**, **PG3**, **PG4** and **PG5** with a fixed amount of P3HT (50 mg ml^{-1}) and varied the graphene quantity as 0, 4.8, 10.7, 19.4, 25.4 and 31.7 wt%, respectively. Note that the final graphene concentration in the blend solution was estimated after subtracting the undispersed/thick graphene from the total weight of the graphene added.

Preparation of electrospun composite nanofibers

The aligned electrospun P3HT/graphene composite nanofibers were produced using a two-fluid coaxial electrospinning technique with a modified collector, as shown in Fig.1. The core and shell precursor solutions in the two syringes were used for the preparation of nanofibers. Note that each syringe was connected to the separate needles for the two-fluid coaxial electrospinning system. P3HT/graphene blend solution (graphene loading concentration summarized in Table 1) as the core solution and PEO in chlorobenzene (50 mg mL^{-1}; 10 wt% of TBAP to increase conductivity and stabilize the cone-jet) as the shell solution were fed into the coaxial capillaries by two syringe pumps (KD Scientific Model 100, USA). The feeding rates of the P3HT/graphene solution (core flow) was at 0.1 ml h^{-1} and the PEO solution (shell flow) was at 1.0 ml h^{-1}, respectively. The tip of the core needle was connected to a high-voltage power supply (chargemaster CH30P SIMCO, USA) with the operating voltage of 5.8~7.2 kV and working distance of 13 cm. The collector made of electrically charged conductive aluminium disk (diameter in 7 cm) with a rectangular hole (4 cm in length and gap width in 1 cm) was placed to collect the aligned nanofibers. The stable cone-jet spinning mode in the electrospinning process system was monitored by a CCD camera (Xli 3 M USB2.0 CCD camera, USA) and macro video zoom lens (OPTEM MVZL, USA) for obtaining uniform and aligned nanofibers. All experiments were carried out under an ambient environment.

Characterization of the fabricated nanofibers

Transmission Electron Microscopy (TEM, JEM-1230, JEOL) operated at a 100 kV accelerating voltage was used to characterize nanofibers and thin films. Photoluminescence (PL) spectra was obtained by a SPEX FluoroLog-3 spectrofluorometer system (Horiba Jobin Yvon). A laser scanning two-photon and confocal microscope equipped with illumination source (wavelength at 561 nm) and detector (in a wavelength range of 650-700 nm) was used in the imaging mode. The thickness of polymer composite film was determined with a microFigure measuring instrument (Surfcorder ET3000, Kosaka Laboratory Ltd.).

Device fabrication and Characterization

For the FET device fabrication shown in Fig. 1, source and drain electrodes were prepared by the thermal evaporation of 100 nm Au through the shadow mask (chamber pressure = 10^{-6} torr; evaporation rate = 0.2 Å s^{-1}). The standard channel length and width were 25 and 1500 nm, respectively. For the purpose of comparison, thin film devices were produced by spin-coating the P3HT/graphene blend solution at 1000 rpm for 60 s and then depositing the top electrode under the same experimental procedure. Composite FET electrical characterizations were performed at room temperature under nitrogen atmosphere by employing a probe station connected to a Keithley 4200 semiconductor parametric analyzer. The field effect mobility (μ) of thin film FET was calculated using eq.(1) that describes the drain current (I_d) in the saturation region (at high gate voltage (V_g)), as given by

$$I_d = \frac{WC_{ox}}{2L}\mu(V_g - V_{th})^2 \qquad (1)$$

where W, L and C_{ox} are channel width, length, and capacitance per unit area of the SiO$_2$ gate dielectric, respectively. The mobility was calculated from the slope of a line fitted to the straight line portion of the transfer characteristics (I_d -V_g) plotted as $I_d^{1/2}$-V_g, where the intercept with abscissa gives V_{th}. However, the performance of nanofiber FET was determined

2 | *J. Mater. Chem. C*, 2015, **XX**, X-X

This journal is © The Royal Society of Chemistry 2015

Table 1 FET performances based on active layer using the P3HT/graphene composite nanofibers or thin films.

Composite FET	Samples	Graphene content (wt%)	μ (cm^{2}V^{-1}s^{-1})	I_{ON}/I_{OFF}	V_{th} (V)
Electrospun nanofiber (**ES-PGX**)	**ES-PG0**	0	0.09	2.38×10^4	3.67
	ES-PG1	4.8	0.19	8.61×10^4	4.44
	ES-PG2	10.7	0.46	4.22×10^4	5.21
	ES-PG3	19.4	0.81	6.49×10^5	5.87
	ES-PG4	25.4	1.82	5.88×10^4	6.27
	ES-PG5	31.7	1.64	1.89×10^3	7.80
Spin-coating thin film (**SC-PGX**)	**SC-PG0**	0	0.02	2.73×10^3	19.11
	SC-PG1	4.8	0.06	4.99×10^3	19.39
	SC-PG2	10.7	0.09	1.41×10^3	23.96
	SC-PG3	19.4	0.12	1.00×10^2	33.08
	SC-PG4	25.4	0.10	5.20×10	34.65
	SC-PG5	31.7	0.14	3.86×10	34.91

Note: The data of FET performances were averaged from 10 device cells in two different batches.

by modified equation. Since the semiconducting cylinder over a planar dielectric layer can be approximated as a coaxial capacitor for nanofiber-based FET devices, the nanofiber capacitance per unit length (C/L) with respect to the back gate is described by $2\pi\varepsilon\varepsilon_o/\ln(2h/r)$ where r, h, and ε are the radius of the nanofiber, the thickness (300 nm) and average dielectric constant (~2.5) of dielectric layer, respectively.

Results and discussion

Fiber morphology

The P3HT/graphene composite nanofibers fabricated using the two-fluid coaxial electrospinning were immersed in deionized water for 1 h to extract the PEO shell layer and dried under vacuum for 12 h. The aligned-degree of the prepared nanofibers was determined from the distribution of the angle between the long axis of nanofibers and the normal to the edge of two parallel electrodes. The angle distribution shown in Fig. 2 exhibits a narrow range of 0-15° (estimated from more than 30 nanofibers), suggesting the superior alignment of the ES nanofibers. The average diameters of P3HT/graphene composite nanofibers are 186 (**ES-PG1**), 181 (**ES-PG2**), 184 (**ES-PG3**), 188 (**ES-PG4**), and 191 (**ES-PG5**) nm, respectively. Note that the diameter distribution of **ES-PG4** is shown in Fig S1 of ESI†.

The dispersion and morphology of P3HT/graphene composite nanofibers (**ES-PGX**) and thin films (**SC-PGX**) were studied by TEM analysis, and the corresponding images are shown in Fig. 3 (**PG0**, **PG2** and **PG5**) and Fig. S2 (**PG1**, **PG3** and **PG4**) of ESI†. As expected, the addition of graphene in the P3HT solution may change the conductivity of the polymer solution, leading to different textural morphology of the graphene-loaded composite nanofibers compared to that of the parent P3HT. When graphene is introduced into the P3HT matrix, its flakes appear dark phase due to the high electron density. At an optimum condition, uniform and homogeneous nanofibers or thin films were readily obtained when graphene flakes were used as nanofillers. Furthermore, when the graphene composition enhances, the increase of graphene flake

size is observed in composite thin films or nanofibers due to the graphene crumpling or restacking during processing. The average sizes of graphene flakes in the composite thin films are around 21.8±8.1 (**SC-PG1**), 31.5±5.1 (**SC-PG2**), 36.4±9.6 (**SC-PG3**), 48.5±8.6 (**SC-PG4**), and 50.9±11.8 (**SC-PG5**) nm; that of graphene flakes in the nanofibers are 12.1±2.1 (**ES-PG1**), 15.2±3.0 (**ES-PG2**), 17.0±1.7 (**ES-PG3**), 18.2±2.1 (**ES-PG4**), and 19.4±1.7 (**ES-PG5**) nm. The much smaller graphene size in the nanofibers compared to that of the spin-coated film, suggesting the significance of the geometrical confinement of the former.
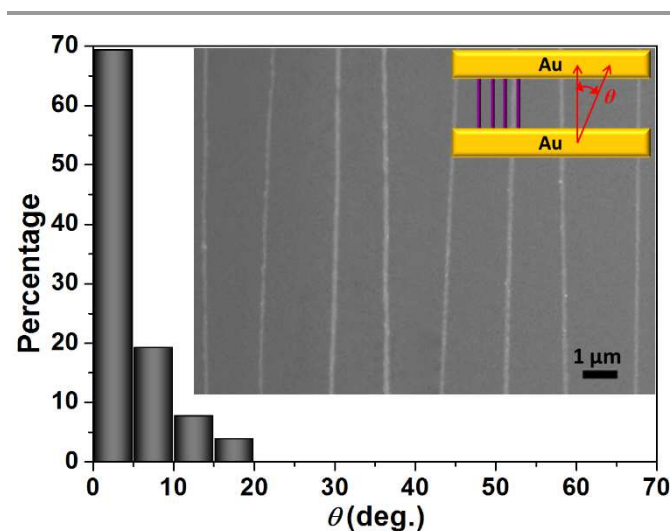
Fig. 2 Distribution diagram of angle between the long axis of the prepared electrospun nanofibers and the normal to the edges of two electrodes. The inset Figure shows SEM image of the P3HT/graphene aligned nanofibers.

The cross-section TEM images in the high magnification of composite nanofiber are shown in the inset of Fig. 3(a)-(c) and Fig. S2(a)-(c) of ESI†. The images show that the individual

This journal is © The Royal Society of Chemistry 2012

J. Mater. Chem. C, 2015, **XX**, X-X | **3**

graphene is well embedded and confined in the composite nanofiber matrix. On the other hand, the pristine P3HT spin-coated thin film (**SC-PG0**) features a grain-like structures (Fig. 3(d)) and P3HT/graphene composite thin films (**SC-PG1~SC-PG5**) show the presence of the aggregated graphene on the P3HT film (Fig. 3 (d)-(f) and Fig. S2(d)-(f) of ESI†). In addition, the thin film surface looks to be more graphene aggregates embedded as the content of graphene increases.
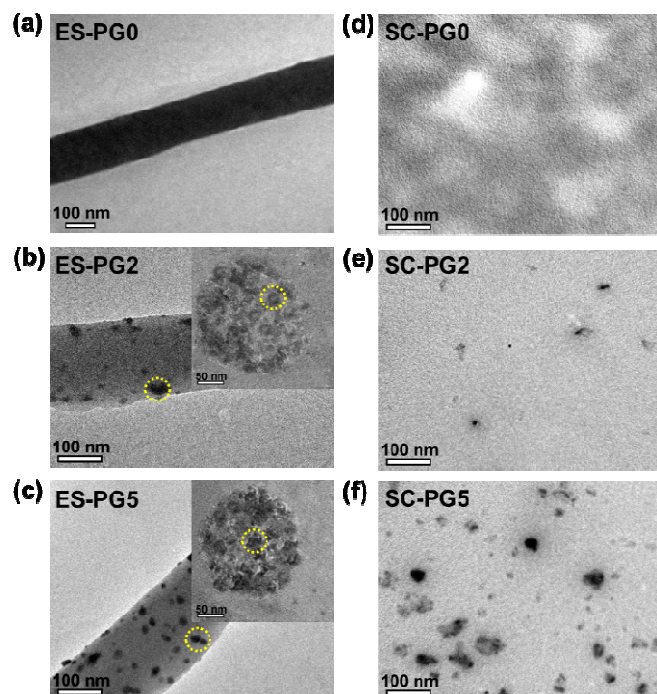
Fig. 3 TEM images of the prepared composites: nanofibers- (a) **ES-PG0**, (b) **ES-PG2** and (c) **ES-PG5** (The graphene is marked in yellow dot circle.); thin films-(d) **SC-PG0**, (e) **SC-PG2** and (f) **SC-PG5**. The insets of (a), (b) and (c) show the cross-section TEM images of the prepared composite nanofibers.

The absorption spectra of pristine P3HT, P3HT/graphene composite nanofibers (**ES-PGX**) and spin-coated thin films (**SC-PGX**) are shown in Fig. S3 of ESI†. In the spectra of nanofibers or thin films, no significant changes in overall absorption features, indicating no ground state interaction occurred between P3HT and graphene.[39] However, there is a slight red-shifting of 6 nm on the absorption peak of **ES-PGX** nanofibers compared to **SC-PGX** thin films, suggesting the higher crystalline P3HT domains with improved π-π stacking during electrospinning. Fig. 4 shows the photoluminescence (PL) emission spectra of the prepared electrospun nanofibers and spin-coated films. Pristine P3HT nanofiber (**ES-PG0**) and thin film (**SC-PG0**) exhibit a strong PL emission between 600 and 800 nm with the excitation at 550 nm. However, the PL intensity is significantly reduced with the increased graphene composition, indicating that the PL quenching by graphene on the emission of P3HT.[40-42] It suggests that efficient photo-induced charge transfer occurs between the P3HT donor and graphene acceptor.

Confocal laser microscopy can also give another insight on the uniformity of the prepared composites. Fig. 5 and Fig. S4 of

ESI† show the PL imaging of P3HT and the graphene composites **ES-PGX** and **SC-PGX**. The confocal images of pristine P3HT nanofibers (Fig. 5(a)) and thin film (Fig. 5(d)) show a homogenous emission without any pattern. Since electroactive blends or composites induce additional charge carriers in neighboring polymers, large areas that appear darker are subjected to the more exiction-polaron quenching. With increasing the graphene composition, the overall PL intensity in the composite images (Fig. 5(b)-(c) and its insets) decreases homogenously, indicating the homogeneous distribution of graphene in the P3HT composite nanofibers. On the other hand, the P3HT/graphene thin film of **SC-PGX** shows a significantly decrease on PL intensity as the graphene composition exceeds 10.7 wt%, as shown in Fig. S4 of ESI and Fig. 5(f). In addition, the insets of Fig. 5(e)-(f) show the non-emissive and dark areas of composite films, which increase in density with increasing graphene blending. Thus, PL quenching mainly occurs in the graphene rich region, and darker areas can be assigned to be with a high graphene loading. The above result suggests that graphene blending into P3HT significantly affects the charge generation process.
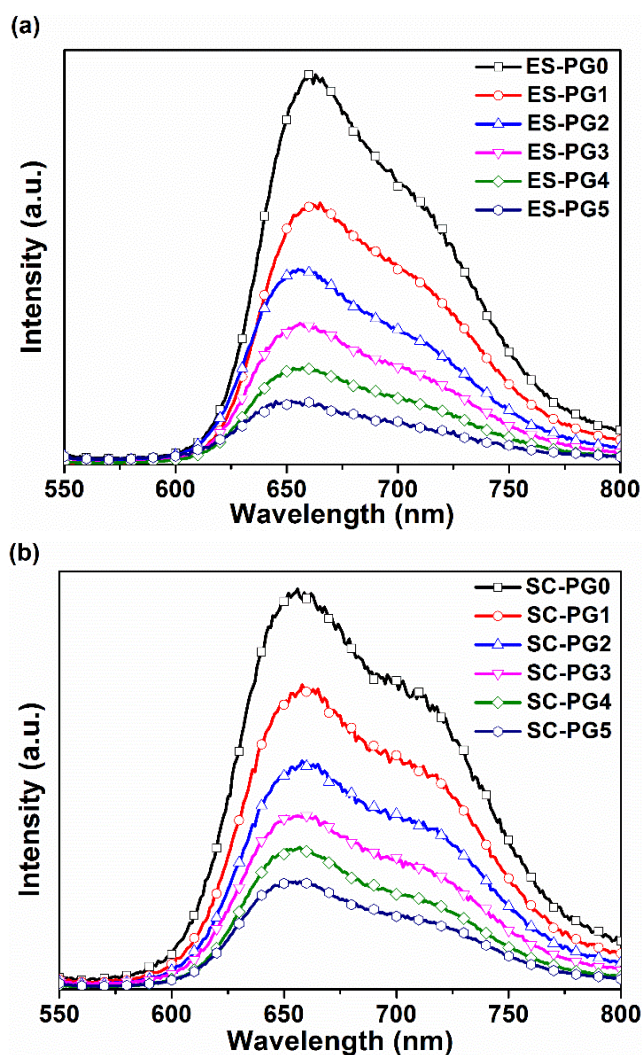
Fig. 4 PL emission spectra of the P3HT/graphene composites: (a) **ES-PGX** nanofibers and (b) **SC-PGX** thin films with different graphene contents.

4 | *J. Mater. Chem. C*, 2015, **XX**, X-X

This journal is © The Royal Society of Chemistry 2015
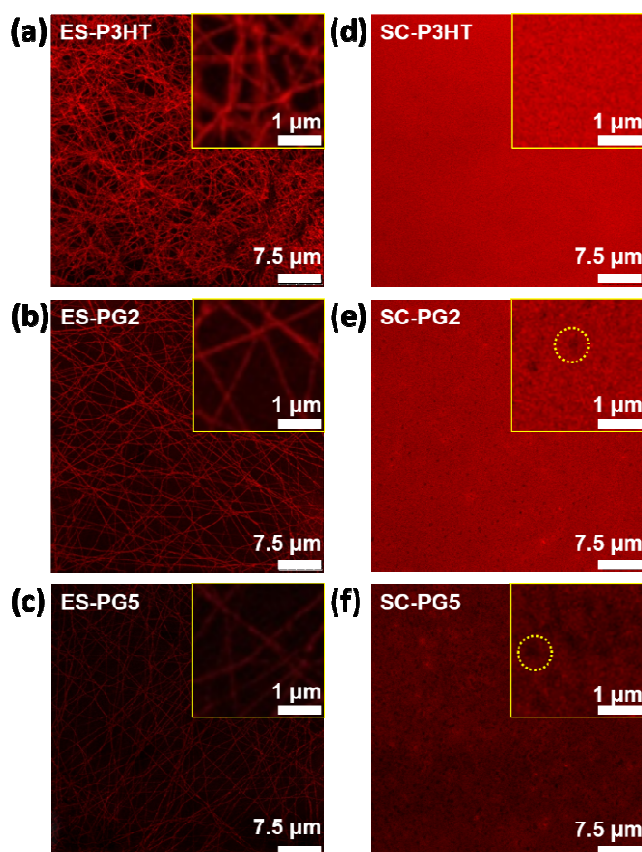
Fig. 5 Confocal fluorescence image of the prepared composites: nanofibers-(a) **ES-PG0**, (b) **ES-PG2** and (c) **ES-PG5**; thin films-(d) **SC-PG0**, (e) **SC-PG2** and (f) **SC-PG5**. The insets show the magnified images (the graphene rich domains are marked in the yellow dot circle).

The electrical characteristics of the **ES-PGX** and **SC-PGX** composites were studied using the bottom-gate top-contact (BGTC) FET device configuration associated with the ODTS-treated dielectric layer. Fig. 6(a) and 6(b) show the output characteristics of composite nanofiber (**ES-PG4**) and thin film (**SC-PG4**), respectively. The inset of Fig. 6(a) shows the SEM image of typical single composite nanofiber-based FET. A clear transition is observed from linear to saturation region. At a given V_g, I_d initially increases and then saturates until pinch-off in the accumulation layer in the interface between the composite semiconductor and SiO_2 dielectric. Fig. 7 shows the transfer characteristics of the corresponding P3HT/graphene composites based FET. Both nanofibers and thin film-based composite FET present a clear p-type behavior under the negative V_g. Device performances such as field effect mobility (μ), current ON/OFF ratio (I_{ON}/I_{OFF}), and threshold voltage (V_{th}) were subsequently extracted from the transfer characteristics in saturation, as summarized in Table 1. The pristine P3HT nanofiber (**ES-PG0**) and thin film (**SC-PG0**) control devices have the FET mobilities of 0.09 and 0.02 cm^2 V^{-1} s^{-1}, respectively, similar to those reported previously.[18] Notably, both I_{ON} and I_{OFF} increase by several orders of magnitude after incorporating with graphene. In particular, the effective μ in the composite nanofibers (**PG4**, with 25.4 % of graphene composition) based FET is increased by an order of magnitude while maintaining the large I_{ON}/I_{OFF} similar to that of the P3HT based FET. As the graphene composition is

increased further, the FET mobility is slightly decreased and the I_{ON}/I_{OFF} is also reduced, due to the graphene aggregation. It suggests that graphene can facilitate the charge transport within the conductance channel and graphene act as preferential routes leading the carriers transport much easier in P3HT/graphene composite than that of pristine P3HT.[33-38]
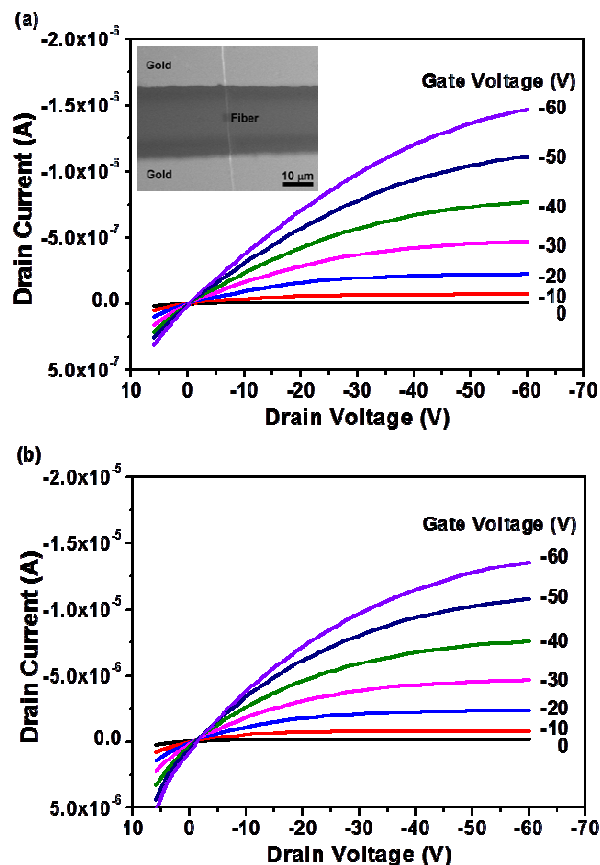
Fig. 6 Output characteristics of P3HT/graphene composites based FET devices: (a) nanofiber (**ES-PG4**) and (b) thin film (**SC-PG4**). The inset of (a) shows the SEM image of the typical FET device prepared from the **ES-PG4** nanofibers.

The schematic illustration for the charge carrier transport within the P3HT/graphene composite nanofiber and thin film channels are shown in Fig. 8. The graphene is randomly distributed within the P3HT matrix and the numbers of graphene located in the source/drain gap is proportional to the concentration of graphene. In the composites, the graphene behave as the electronically conducting bridge between the P3HT domains.[33-38] The positive-shifted V_{th} and increased μ are due to the reduced active conducting channel length provided by graphene in the FET and well-matching HOMO level to the Au electrode, presenting a favorable pathway for charge transport. Efficient carrier conduction can induce a more efficient hole transport from the Au electrode to the HOMO level of P3HT/graphene composites. Thus, the I_d of FET enhances evidently as the graphene composition is increased. However, the I_{OFF} of nanofiber FET remains unchanged (~10^{-11} A) for the low graphene loading concentration (**ES-PG1**~ **ES-PG3**). Note that a gently increased I_{OFF} is observed when the

This journal is © The Royal Society of Chemistry 2012

J. Mater. Chem. C, 2015, **XX**, X-X | 5
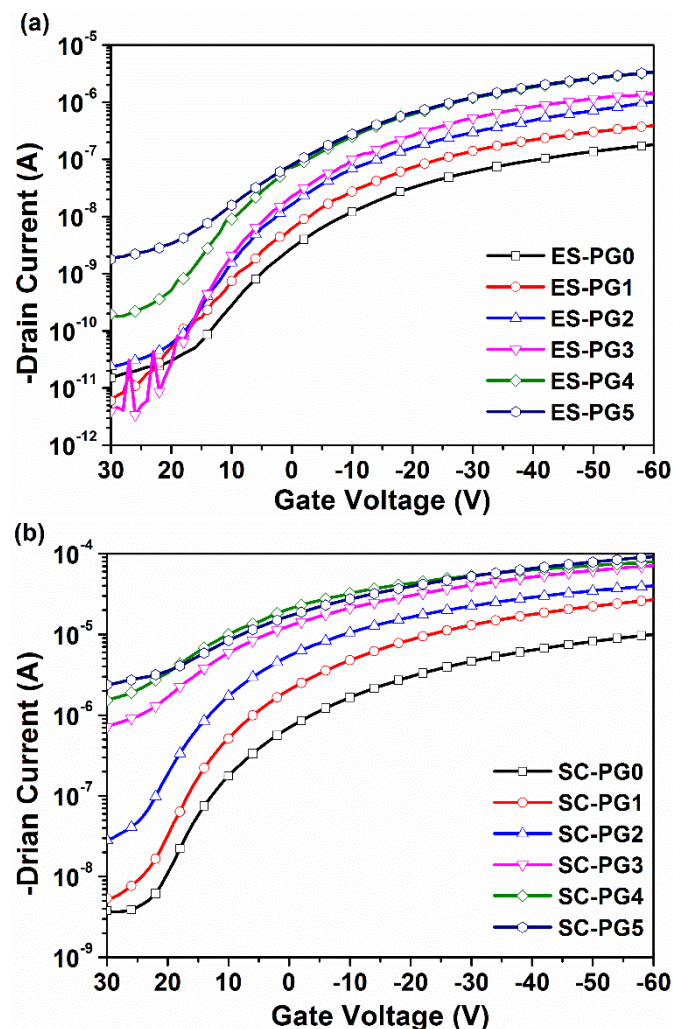
Fig. 7 Transfer characteristics of P3HT/graphene composites based FET: (a) nanofiber and (b) thin film.
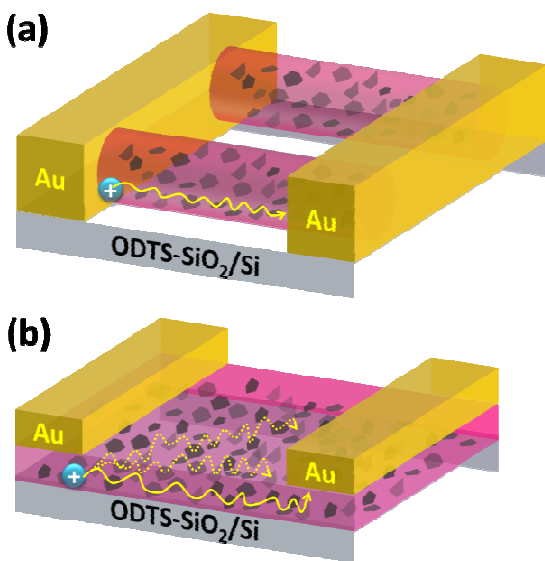
Fig. 8 Illustration of carrier transporting routes in P3HT/graphene composites: (a) nanofiber and (b) thin film.

graphene composition is more than 25.4% (**ES-PG4** for 10^{-10} A; **ES-PG5** for 10^{-9} A). But an obviously increase in I_{OFF} of composite thin film (**SC-PGX**) based FET is observed in the case of graphene composition exceeding 10.7%. This difference of the critical graphene concentration may be referred to that the composite thin film based FET probably has the percolation network between the source/drain electrodes at a low V_g bias (Fig. 8(b)), leading to a high I_{OFF} leakage. On the other hand, the charge transport in composite nanofibers based device is confined in one-dimension nanochannel array when the chains are aligned parallel to the transport direction (Fig. 8(a)). P3HT/graphene composite nanofibers based FET exhibit a much higher I_{ON} to compensate the loss from the enhancement in I_{OFF}, giving an I_{ON}/I_{OFF} ~100 times larger than those of composite thin films. Remarkably, the **ES-PG4** FET have a highest μ of 1.82 $cm^2\,V^{-1}\,s^{-1}$ and moderately high I_{ON}/I_{OFF} of 5.88×10^4. It suggests that one-dimensional nanostructure could result in an enhanced π-π molecular packing with highly ordered orientation and reduced grain boundary during the strong stretching force of electrospinning, thereby increasing μ as compared with those of spin-coated thin film devices.[18-26] For the test of the long term environmental stability, composite nanofibers based FET were place in an uncontrolled ambient air with a relative humidity within the range of 50-70% at 25°C. The environmental stability was investigated by selective time-varying transfer curves of the test FET, as shown in Fig. 9. A moderate change on the device characteristic as the FET mobility and I_{ON}/I_{OFF} reduces from 1.82 to 0.75 $cm^2\,V^{-1}\,s^{-1}$ and from 5.88×10^4 to 2.09×10^3, respectively, after exposure to air for 720 h. In comparison, the FET using pristine P3HT nanofibers exhibited poor air stability. The mobility and I_{ON}/I_{OFF} of this FET decayed rapidly from 0.09 to 2.45×10^{-4} $cm^2\,V^{-1}\,s^{-1}$ for mobility and 2.38×10^4 to 7.46×10 for I_{ON}/I_{OFF} after exposed to air for 24 h. Furthermore, the literature clearly evidenced that pristine P3HT lost the transistor performance after exposed to air for 1 day under ambient atmosphere.[20] In contrast with the FET of pristine P3HT nanofibers, the good stability of the **ES-PG4** can be explained by the characteristic of graphene. Graphene is a radical scavenger and an efficient quencher to prevent P3HT oxidation. Identical results have been reported by Manceau et al. concerning P3HT/PCBM blending system.[43, 44] These results indicate that 1D composites based nanofiber devices offer advantageous over the conventional thin film ones and provide a simple strategy to produce high performance FET devices.
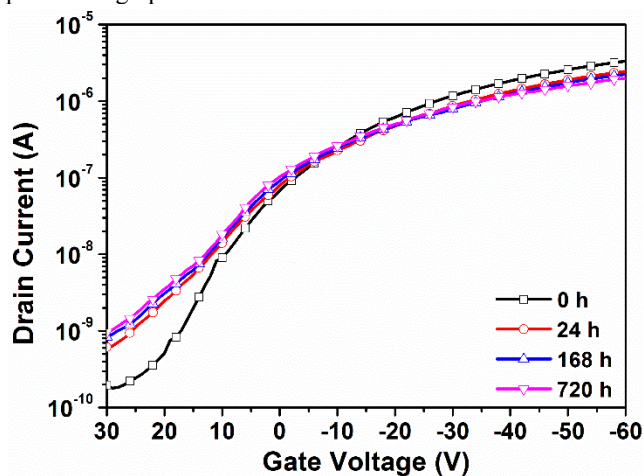
Fig. 9 Transfer curves of **ES-PG4** nanofibers based FET under air with different exposure times.

Conclusions

We have successfully fabricated high performance FET using aligned electrospun nanofibers of P3HT/graphene composite. The experimental results showed that the geometrical confinement of nanofibers could limit the graphene aggregation and promoted the carrier transport to produce high carrier mobility. The mobilities of composite nanofibers-based FET were distinctly enhanced with increasing the graphene composition from 0.09 cm^2 V^{-1} s^{-1} for pristine P3HT (**ES-PG0**) to 1.82 cm^2 V^{-1} s^{-1} for 25.4 % graphene loading (**ES-PG4**) without degrading I_{ON}/I_{OFF} (as high as at least 10^4). This outstanding enhancement could be ascribed to that the graphene acted as preferential routes for facilitating charge transport in the semiconducting composite layer. In addition, the prepared aligned electrospun nanofibers based FET revealed around one order of magnitude higher on the carrier mobility than spin-coated thin films due to the confined carrier transport. The strategy combined with the 1D nanofiber structures for tuning effective charge transport and nanocomposite for bridging the semiconducting channel could improve the electrical properties for their applications in FET or other electronic devices.

Acknowledgements

Notes and references

1   A. Facchetti, *Chem. Mater.*, 2010, **23**, 733-758.
2   Y.-H. Chou, H.-C. Chang, C.-L. Liu and W.-C. Chen, *Polym. Chem.*, 2015, **6**, 341-352.
3   P. M. Beaujuge and J. R. Reynolds, *Chem. Rev.*, 2010, **110**, 268-320.
4   J. C. Scott and L. D. Bozano, *Adv. Mater.*, 2007, **19**, 1452-1463.
5   M. T. Bernius, M. Inbasekaran, J. O'Brien and W. Wu, *Adv. Mater.*, 2000, **12**, 1737-1750.
6   R. H. Friend, R. W. Gymer, A. B. Holmes, J. H. Burroughes, R. N. Marks, C. Taliani, D. D. C. Bradley, D. A. D. Santos, J. L. Bredas, M. Logdlund and W. R. Salaneck, *Nature*, 1999, **397**, 121-128.
7   S. Günes, H. Neugebauer and N. S. Sariciftci, *Chem. Rev.*, 2007, **107**, 1324-1338.
8   X. Lu, W. Zhang, C. Wang, T.-C. Wen and Y. Wei, *Prog. Polym. Sci.*, 2011, **36**, 671-712.
9   S. Chen, Y. Li and Y. Li, *Polym. Chem.*, 2013, **4**, 5162-5180.
10 H.-C. Chang, C. Lu, C.-L. Liu and W.-C. Chen, *Adv. Mater.*, 2015, **27**, 27-33.
11 S. Agarwal, A. Greiner and J. H. Wendorff, *Prog. Polym. Sci.*, 2013, **38**, 963-991.
12 J. Wu, N. Wang, Y. Zhao and L. Jiang, *J. Mater. Chem. A*, 2013, **1**, 7290-7305.
13 B. Sun, Y. Z. Long, H. D. Zhang, M. M. Li, J. L. Duvail, X. Y. Jiang and H. L. Yin, *Prog. Polym. Sci.*, 2014, **39**, 862-890.
14 B. Sun, Y.-Z. Long, Z.-J. Chen, S.-L. Liu, H.-D. Zhang, J.-C. Zhang and W.-P. Han, *J. Mater. Chem. C*, 2014, **2**, 1209-1219.
15 M. Campoy-Quiles, Y. Ishii, H. Sakai and H. Murata, *Appl. Phys. Lett.*, 2008, **92**, 213305.
16 D. Tu, S. Pagliara, A. Camposeo, L. Persano, R. Cingolani and D. Pisignano, *Nanoscale*, 2010, **2**, 2217-2222.
17 C. J. Lin, J. C. Hsu, J. H. Tsai, C. C. Kuo, W. Y. Lee and W. C. Chen, *Macromol. Chem. Phys.*, 2011, **212**, 2452-2458.
18 J. Y. Chen, C. C. Kuo, C. S. Lai, W. C. Chen and H. L. Chen, *Macromolecules*, 2011, **44**, 2883-2892.
19 P.-Z. Jian, Y.-C. Chiu, H.-S. Sun, T.-Y. Chen, W.-C. Chen and S.-H. Tung, *ACS Appl. Mater. Interfaces*, 2014, **6**, 5506-5515.
20 C. C. Chou, H. C. Wu, C. J. Lin, E. Ghelichkhani and W. C. Chen, *Macromol. Chem. Phys.*, 2013, **214**, 751-760.
21 E. V. Canesi, A. Luzio, B. Saglio, A. Bianco, M. Caironi and C. Bertarelli, *ACS Macro Lett.*, 2012, **1**, 366-369.
22 N. J. Pinto, A. T. Johnson, A. G. MacDiarmid, C. H. Mueller, N. Theofylaktos, D. C. Robinson and F. A. Miranda, *Appl. Phys. Lett.*, 2003, **83**, 4244-4246.
23 D. Li, A. Babel, S. A. Jenekhe and Y. Xia, *Adv. Mater.*, 2004, **16**, 2062-2066.
24 H. Liu, C. H. Reccius and H. G. Craighead, *Appl. Phys. Lett.*, 2005, **87**, 253106.
25 C. Lu, J. Wang, H.-C. Chang, Y.-C. Chiu, H.-Y. Chen, H.-C. Wu, T. Higashihara and W.-C. Chen, *J. Mater. Chem. C*, 2014, **2**, 7489-7493.
26 S. W. Lee, H. J. Lee, J. H. Choi, W. G. Koh, J. M. Myoung, J. H. Hur, J. J. Park, J. H. Cho and U. Jeong, *Nano Lett.*, 2010, **10**, 347-351.
27 N. Roy, R. Sengupta and A. K. Bhowmick, *Prog. Polym. Sci.*, 2012, **37**, 781-819.
28 T. Kuilla, S. Bhadra, D. Yao, N. H. Kim, S. Bose and J. H. Lee, *Prog. Polym. Sci.*, 2010, **35**, 1350-1375.
29 X. Huang, X. Qi, F. Boey and H. Zhang, *Chem. Soc. Rev.*, 2012, **41**, 666-686.
30 X. Qi, C. Tan, J. Wei and H. Zhang, *Nanoscale*, 2013, **5**, 1440-1451.
31 X. Sun, H. Sun, H. Li and H. Peng, *Adv. Mater.*, 2013, **25**, 5153-5176.
32 A. Schlierf, P. Samori and V. Palermo, *J. Mater. Chem. C*, 2014, **2**, 3129-3143.
33 J. Huang, D. R. Hines, B. J. Jung, M. S. Bronsgeest, A. Tunnell, V. Ballarotto, H. E. Katz, M. S. Fuhrer, E. D. Williams and J. Cumings, *Org. Electron.*, 2011, **12**, 1471-1476.
34 S. Tiwari, S. K. Singh and R. Prakash, *J. Nanosci. Nanotechnol.*, 2014, **14**, 2823.
35 M. El Gemayel, S. Haar, F. Liscio, A. Schlierf, G. Melinte, S. Milita, O. Ersen, A. Ciesielski, V. Palermo and P. Samorì, *Adv. Mater.*, 2014, **26**, 4814-4819.
36 M. El Gemayel, A. Narita, L. F. Dossel, R. S. Sundaram, A. Kiersnowski, W. Pisula, M. R. Hansen, A. C. Ferrari, E. Orgiu, X. Feng, K. Mullen and P. Samori, *Nanoscale*, 2014, **6**, 6301-6314.
37 P. Yadav, C. Chanmal, A. Basu, L. Mandal, J. Jog and S. Ogale, *RSC Adv.*, 2013, **3**, 18049-18054.
38 A. Liscio, G. P. Veronese, E. Treossi, F. Suriano, F. Rossella, V. Bellani, R. Rizzoli, P. Samori and V. Palermo, *J. Mater. Chem.*, 2011, **21**, 2924-2931.
39 Q. Liu, Z. F. Liu, X. Y. Zhong, L. Y. Yang, N. Zhang, G. L. Pan, S. G. Yin, Y. Chen and J. Wei, *Adv. Funct. Mater.*, 2009, **19**, 894-904.
40 V. Saini, O. Abdulrazzaq, S. Bourdo, E. Dervishi, A. Petre, V. G. Bairi, T. Mustafa, L. Schnackenberg, T. Viswanathan and A. S. Biris, *J. Appl. Phys.*, 2012, **112**, 054327.

41 Z. Yang, X. Shi, J. Yuan, H. Pu and Y. Liu, *Appl. Surf. Sci.*, 2010, **257**, 138-142.

42 Z. F. Liu, Q. Liu, Y. Huang, Y. F. Ma, S. G. Yin, X. Y. Zhang, W. Sun and Y. S. Chen, *Adv. Mater.*, 2008, **20**, 3924.

43 M. Manceau, S. Chambon, A. Rivaton, J.-L. Gardette, S. Guillerez and N. Lemaître, *Sol. Energy Mater Sol. Cells*, 2010, **94**, 1572-1577.

44 H. Hintz, H. J. Egelhaaf, L. Lüer, J. Hauch, H. Peisert and T. Chassé, *Chem. Mater.*, 2010, **23**, 145-154.

Journal of Materials Chemistry C Accepted Manuscript

8 | *J. Mater. Chem. C*, 2015, **XX**, X-X

A table of contents entry
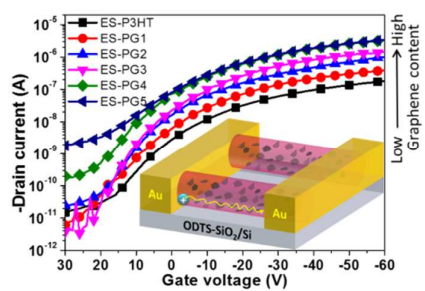
High performance FET was successfully fabricated using aligned electrospun P3HT/graphene composite nanofibers with a highest mobility of 1.82 $cm^2\,V^{-1}\,s^{-1}$.